

# Nanophotonic Crescent Moon Structures with Sharp Edge for Ultrasensitive Biomolecular Detection by Local Electromagnetic Field Enhancement Effect

Yu Lu,<sup>†</sup> Gang L. Liu,<sup>†</sup> Jaeyoun Kim, Yara X. Mejia, and Luke P. Lee\*

Berkeley Sensor and Actuator Center, Department of Bioengineering,  
University of California-Berkeley, Berkeley, California 94720

Received October 26, 2004; Revised Manuscript Received November 18, 2004

## ABSTRACT

We present novel gold nanophotonic crescent moon structures with a sub-10 nm sharp edge, which can enhance local electromagnetic field at the edge area. The formation of unconventional nanophotonic crescent moon structure is accomplished by using a sacrificial nanosphere template and conventional thin film deposition method, which allows an effective batch nanofabrication and precise controls of nanostructure shapes. Unique multiple scattering peaks are observed in a single gold nanocrescent moon with dark-field white light illumination. A 785 nm near-infrared (NIR) diode laser was used as the excitation source to induce the amplified scattering field on the sharp edge of the single gold nanocrescent moon. The Raman scattering spectrum of Rhodamine 6G molecules adsorbed on the single gold nanocrescent moon are characterized, and the Raman enhancement factor of single gold nanocrescent moon is estimated larger than  $10^{10}$ , which suggests the potential applications of gold nanocrescent moons in ultrasensitive biomolecular detection and cellular imaging using surface enhanced Raman spectroscopy.

Raman spectroscopy is a label-free technique desired for ultrasensitive biomolecule detection and molecular dynamic study because it acquires the unique signatures of each molecule, the vibrational peaks of chemical bonds.<sup>1,2</sup> Surface enhanced Raman scattering (SERS) further improves the sensitivity by amplifying the original Raman scattering intensity for several or even tens of orders of magnitude.<sup>3</sup> Spherical gold and silver nanoparticles have been extensively reported as the substrate in SERS-based molecule detection<sup>4–10</sup> due to their advantages in local scattering field enhancing, surface chemical modifications, biocompatibility, and well-established chemical synthesis process. The intrinsic plasmon resonance of single nanospheres and the plasmon coupling between adjacent nanospheres are considered as the key and necessary conditions for local field enhancing.<sup>11,12</sup> The optimal SERS substrate of spherical nanoparticle assemblies depends on the size, the local dielectric environment and the interparticle distance.<sup>13,14</sup> In conventional chemical synthesis or batch fabrications, the interparticle distance is difficult to control due to the stochastic distribution of the nanospheres on a substrate. Most recently, several groups

have developed nonspherical and reduced-symmetry nanostructures as potential SERS substrates.<sup>15–20</sup> Differing from spherical nanoparticle SERS substrates that rely on interparticle coupling, these unconventional nanostructures are proposed as independent SERS substrates to enhance local scattering field. Among them, nanotip has been experimentally used in local field enhancement, SERS spectroscopy and imaging in which the nanotip provides not only the large local field enhancement but also the high spatial resolution since most SERS signal is generated from the tip area.<sup>15–17</sup> Other cross-sectional ring-like nanostructures such as nanorings,<sup>18</sup> nano half-shells,<sup>19</sup> and nanocups<sup>20</sup> also have been demonstrated and proposed for SERS applications.

In contrast to the previous work, our gold nanocrescent moon has the features of both nanotip and nanoring which allow local electromagnetic field enhancement (Figure 1a). In cross-sectional view, the shape of the nanocrescent moon resembles a crescent nanomoon with sharp tips, so the sharp edge of the gold nanocrescent moon has the rotational analogy to a sharp gold tip and it expands the SERS “hot site” from a tip to a circular line (i.e., a group of nanotips) as shown in Figure 1b. In the top view the shape of the nanocrescent moon resembles a nanoring with a higher sharpness than the previously demonstrated nanoring,<sup>18</sup> so

\* Corresponding author. E-mail: lplee@socrates.berkeley.edu

<sup>†</sup> The first two authors contributed equally.

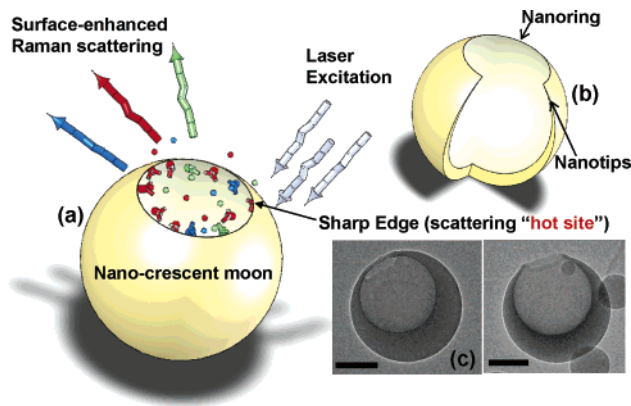


**Figure 1.** Gold nanocrescent moons with sharp edges. (a) Conceptual schematics of a nanocrescent moon SERS substrate. The gold surface can be functionalized with biomolecular linker to recognize specific biomolecules. The sharp edge of the nanocrescent moon can enhance the Raman scattering intensity so that the biomolecules on it can be detected. (b) Geometrical schematics of a nanocrescent moon. A gold nanocrescent moon with sharp edges integrates the geometric features of nanoring and nanotips. (c) Transmission electron microscope images of two nanocrescent moons. Shown nanocrescent moons are both of 300 nm inner-diameter, 100 nm-bottom-thickness, but with different orientations. The scale bars are 100 nm.

the circular sharp edge of the nanocrescent moon can have a stronger field emitting or “antenna” effect.<sup>15</sup>

In this paper the gold nanophotonic crescent moons with sub-10 nm sharp edges as shown in Figure 1c are designed, fabricated, and characterized. We observed multiple scattering peaks of single gold nanocrescent moons from the visible light to NIR region. A 785 nm diode laser excites the single gold nanocrescent moon, and this excited “hot spot” is utilized to detect the SERS spectra of Rhodamine 6G (R6G) molecules with the enhancement factor larger than  $10^{10}$ .

The gold nanocrescent moons are fabricated by rotational deposition of a thin gold layer on polymer nanospheres at certain angles and subsequent dissolution of the sacrificial nanosphere templates as shown in Figure 2.<sup>21</sup> Though the nanocrescent moons with certain dimension are studied here, the inner diameter and thickness of nanocrescent moons can be controlled in the fabrication by choosing the size of sacrificial nanosphere templates as well as the gold deposition thickness and angle. The structures of the nanocrescent moons maintain their original shape and did not collapse during the process of dissolving the sacrificial nanosphere templates or redistributing on a surface for imaging.

Several groups demonstrated significant field enhancing effect by nanotip and nanoring in their numerical simulations and experiments.<sup>17,18</sup> Because our nanocrescent moons have the geometrical features of both nanotip and nanoring on the sharp edge area, we can expect an excellent local field enhancement from that area. Figure 3 shows the simulated electric field amplitude on a sharp-edged gold nanocrescent moon (300 nm inner diameter and 100 nm bottom thickness) with a 785 nm NIR laser excitation. To calculate the field enhancement factor, we numerically solve the 2-D Helmholtz equations using finite element method. The computation

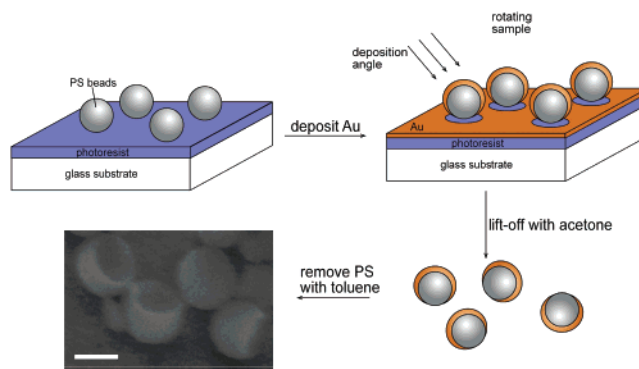


**Figure 2.** Fabrication procedure of gold nanocrescent moons. (a) Casting a monolayer of spherical polystyrene colloids on a photoresist coated glass substrates. (b) Coating a gold layer on the surfaces of polystyrene colloids by electron beam evaporation. The sample is kept rotating at a certain angle with respect to the gold target during deposition. The shape of the nanocrescent moons depends on the deposition angle in addition to the size of the polystyrene spheres. (c) Lift-off of the gold-coated polystyrene spheres from the substrate. (d) Scanning electron microscopy of gold nanocrescent moons. The dissolution of the colloidal particles releases the nanocrescent moons into a suspension. The nanocrescent moons are then collect and placed on a substrate. For the convenience of demonstration in SEM, the shown nanocrescent moons were not subject to dilution in water like the nanocrescent moons used in our optical experiments. The scale bar is 200 nm.

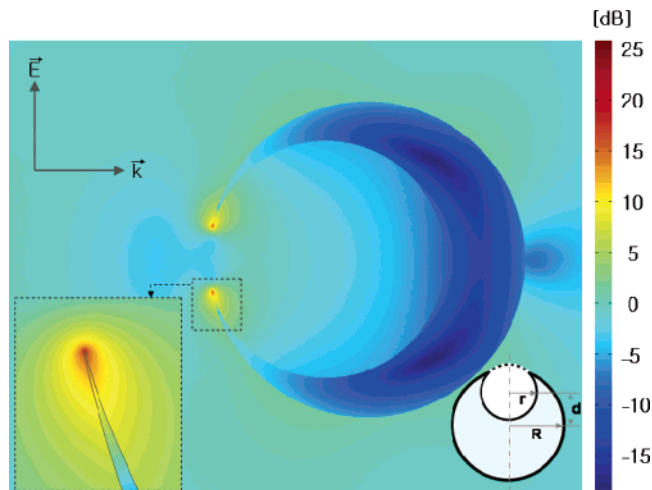


**Figure 3.** Local electric field amplitude distribution of a nanocrescent moon at one of its scattering peak wavelengths (785 nm). The geometry of the nanocrescent moon is shown in the inset schematics where  $r$  is the inner radius,  $R$  is the outer radius, and  $d$  is the center–center distance as shown as two partially overlapping circles. For this nanocrescent moon,  $r = 150$  nm,  $R = 200$  nm,  $d = 51$  nm. The shown field amplitude is normalized with respect to the incident field amplitude. The direction of light incidence is from left to right.

domain is a  $3 \mu\text{m} \times 6 \mu\text{m}$  rectangle with the low-reflection, absorptive boundary condition applied to all four domain boundaries. The computational grid is generated using triangular elements. An adaptive algorithm is employed to automatically reduce the element size in areas of rapidly changing geometry or material properties. We approximate the nanocrescent moon structure in 2-D using two circles as depicted in the inset of Figure 3. The sharp tips of the

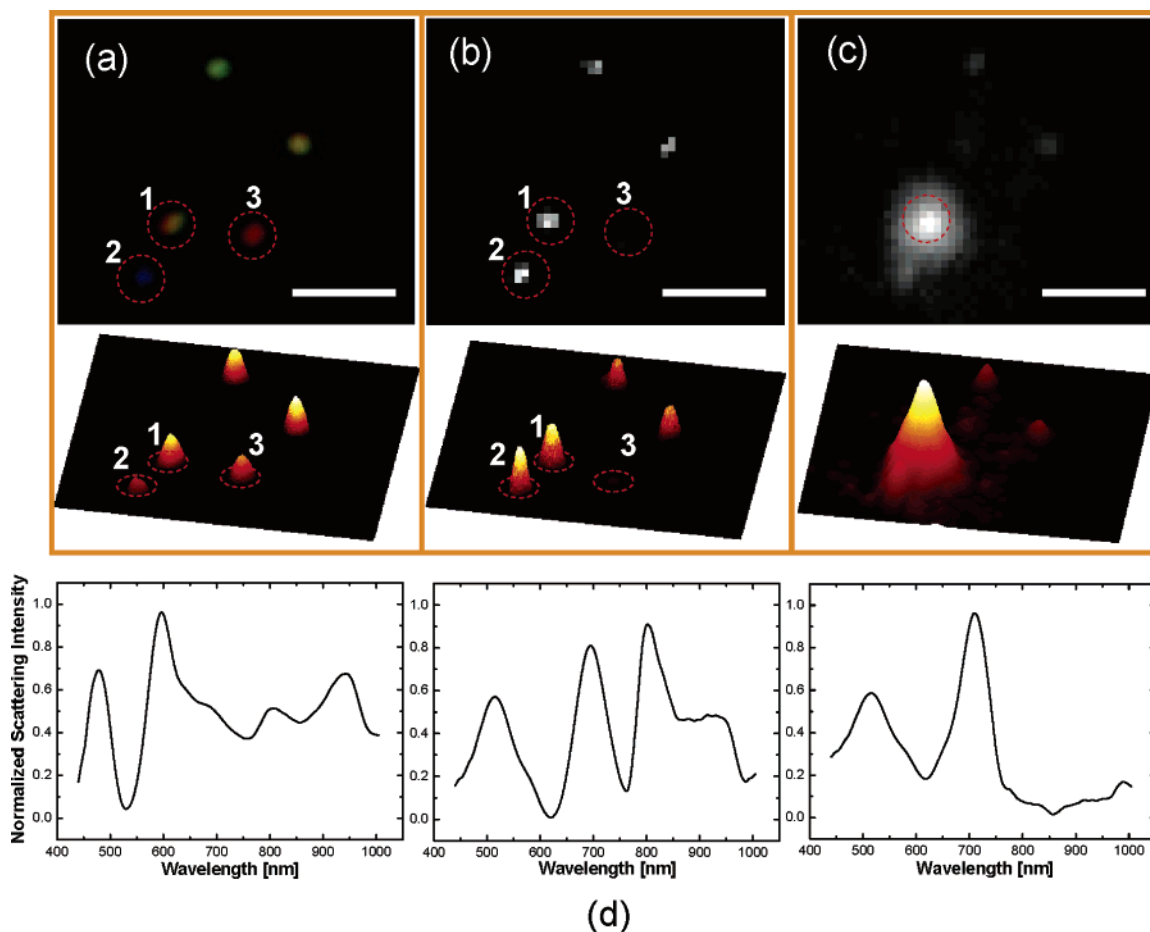


**Figure 4.** Scattering images and spectra of gold nanocrescent moons. (a) True-color dark-field scattering image of gold nanocrescent moons. The laser excitation is turned off and no optical filter is placed in the optical path when taking this image. (b) B/W dark-field scattering image of the same nanocrescent moons at near-infrared region ( $>797$  nm). The laser excitation is still off while two 797 nm long-pass optical filters (optical density  $> 6$ ) are placed in the optical path when taking this image. (c) B/W dark-field scattering image of the same nanocrescent moons with one nanocrescent moon excited by laser. The two optical filters are used. The scale bar is  $10 \mu\text{m}$  in all three images and the contrast of each image is scaled individually. (d) Dark-field scattering spectra of the three marked nanocrescent moons.

nanocrescent moon are rounded with a radius of 0.25 nm to avoid computational anomalies. The wavelength-dependent refractive index of the nanostructures is set to the values of bulk gold reported by Johnson and Christy.<sup>22</sup> We also assume that the nanocrescent moons are in water in accordance with the experiments. As shown in Figure 3, the incident wave is polarized transverse magnetic with respect to the nanocrescent moon. The effect of retardation is fully realized in the simulations. The enhancement factor is determined from the amplitude ratio between the calculated nanocrescent moon near-field and the incident field. The sharp edge area (two sharp tips in the two-dimensional simulation) exhibits the highest level of field enhancement as expected. At the wavelength of maximum field enhancement, the enhancement factor reaches  $\sim 10^{2.6}$ . Since the Raman enhancement factor is proportional to the fourth power of the field amplitude enhancement,<sup>12</sup> the Raman enhancement factor of single gold nanocrescent moon could be up to  $10^{11}$  at the shown resonant wavelength. While the nanocrescent moon shows scattering peak within the wavelength region from 700 to 900 nm, no scattering peaks are found in the

simulation for a nanosphere of the similar size within this wavelength region.

The nanocrescent moons redistributed on a cleaned glass slide are visualized in the dark-field scattering image (Figure 4a; note no optical filter is used when taking the true color image).<sup>23</sup> Figure 4d shows the measured scattering spectra of the three marked nanocrescent moons in Figure 4a. Multiple scattering peaks exist for all the nanocrescent moons in the scattering spectra, but only nanocrescent moons 1 and 2 have peaks with wavelengths longer than 750 nm. Figure 4b shows the dark-field scattering image of the same nanocrescent moons as shown in Figure 4a, but the image is taken by a back-illuminated B/W camera (quantum efficiency  $> 95\%$ , Cascade 512B, Roper Scientific, NJ), and two 797 nm long-pass optical filters (Omega Filters, VT) are used. It is interesting to notice in the 3D surface plots of Figure 4a and 4b that the relative ratio of scattering intensities from three marked nanocrescent moons are different over the whole white light spectrum (Figure 4a) and in the near-infrared light region (Figure 4b). The relative intensity ratio also corresponds to their scattering spectra in Figure 4d. For

example, nanocrescent moon 3 has higher overall intensity than nanocrescent moon 2 in the true color image (Figure 4a), whereas nanocrescent moon 3 disappears and nanocrescent moon 2 stands out in the near-infrared image (Figure 4b). Our simulation results indicate that the common scattering peak near 500 nm is clearly originated from the multipolar excitation of surface plasmon resonance around the outer periphery. The multiple peaks in the NIR regime, however, cannot be explained by the multipolar resonance because the intensity of the simulated field along the outer periphery is significantly lower than those near the edges and in the hollow cavity and plays little role in resonance. Considering the high intensity of the electric fields concentrated at and near the edges, it is appropriate to attribute the peaks to the local plasmon resonances in the edge area and their interplay. It is worth noting that the local field enhancement near the sharp edges of nanocrescent moons greatly exceeds the enhancement originated from the same edges with no cylindrical cavity behind them. Currently simulation and theoretical investigations are under way to clarify the origin of this phenomenon.

The 785 nm laser excitation light scattered from a single gold nanocrescent moon is imaged simultaneously with the scattering light from the white light dark-field illumination by the back-illuminated B/W camera, to make sure that the measured Raman scattering spectrum is from the R6G molecules on a single nanocrescent moon. Figure 4c shows that nanocrescent moon 1 is excited by the laser and the fwhm (full width at half max) of the excitation area is  $\sim 2 \mu\text{m}$ . The white-light illumination is only kept on when searching the nanocrescent moons, and it is turned off during Raman spectra acquisition. The laser power delivered on the nanocrescent moon is measured using a photometer (Newport, CA) to be  $\sim 0.8 \text{ mW}$ .

We tested different concentrations of R6G molecules on the same nanocrescent moons in the following way: first we marked the position where the imaged nanocrescent moons are on the glass substrate. A  $1 \mu\text{L}$  droplet of  $1 \text{ nM}$  R6G is then spread on the marked position over an area of about  $10 \text{ mm}^2$ . With the 785 nm laser excitation, the SERS spectra on the chosen single gold nanocrescent moon are taken with a 10-second exposure time and averaged over 5 recordings. At this concentration level, no apparent Raman peaks are visible for over 30 examined nano-crescent moons. Then a  $1 \mu\text{L}$  droplet of  $1 \mu\text{M}$  R6G is placed on the same marked position as before. The same nanocrescent moons examined previously are found under the dark-field microscopy and the SERS spectra on those gold nano-crescent moons are taken again. The Raman peaks are barely seen at this concentration level on some nanocrescent moons. The same procedures with different concentrations are repeated on each of those nanocrescent moons. The SERS spectra of different concentrations of R6G molecules from one of the nanocrescent moon “hot spots” are shown in Figure 5a after baseline corrections. Each Raman spectrum measurement is done under the same acquisition conditions. The peak intensities increase with the concentration of the added R6G droplets and almost saturate after the addition of  $100 \mu\text{M}$

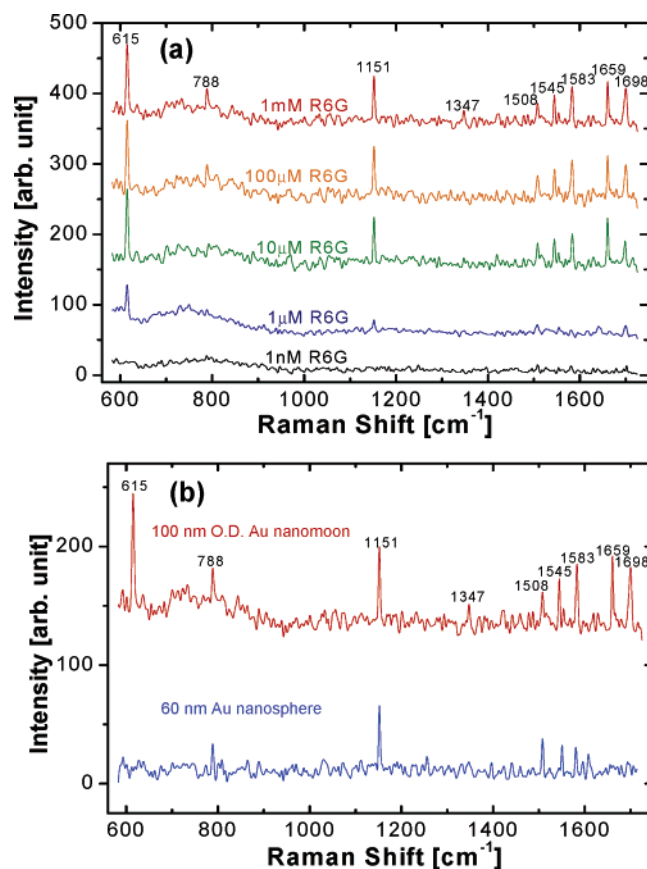


**Figure 5.** SERS spectra of R6G molecules. (a) SERS spectra of different concentrations of R6G molecules adsorbed on a single nanocrescent moon SERS “hot spot”. Baseline signals are corrected for all shown spectra. (b) SERS spectra of  $1 \text{ mM}$  R6G molecules on a single gold nanocrescent moon and  $60 \text{ nm}$  colloidal nanospheres.

R6G droplet. Characteristic peaks are not found in the spectra taken from the areas without nanocrescent moon for all the concentrations. For the purpose of comparison,  $\sim 1 \text{ nM}$   $60 \text{ nm}$  gold nanospheres (Ted Pella, CA) are cast on a glass slide to form clusters, and  $1 \text{ mM}$  R6G molecules adsorbed on the nanosphere cluster are detected using the same procedures. No “hot spots” as good as the shown nanocrescent moons are found for over 30 examined spots on the nanosphere clusters. Figure 5b shows the comparative Raman spectra of  $1 \text{ mM}$  R6G on a gold nanocrescent moon and  $60 \text{ nm}$  gold nanosphere clusters. The R6G Raman spectra from the gold nanocrescent moon contains some peaks with comparatively higher intensities than those in the spectra from the nanosphere clusters, and also contains some peaks that are not visible in the spectra from the nanosphere clusters.

Some nanocrescent moons exhibit different scattering spectra and colors as shown in Figure 4, which is possibly due to the slight difference in their geometries and orientations with respect to the incident light. Since the local field enhancement factor is also related to the orientation of the reduced-symmetry gold nanocrescent moons with respect to the incident field, it could be higher at special orientations. More study is underway on the precise control of the geometry and orientation of nanocrescent moons.

In our experiments, we used a NIR laser (785 nm) as the excitation source instead of a green laser (514 nm) usually used in other nanosphere-based SERS characterizations<sup>5,6</sup> where the scattering peak (plasmon resonance) wavelength is usually around 500–600 nm, except the special inter-coupled nanospheres.<sup>14,24</sup> In addition to the reason of matching the scattering peak wavelength of nanocrescent moons, the near-infrared laser source is more preferable in general bimolecular SERS detection because: (1) it can avoid the excitation of fluorescence from biomolecules; (2) it has a deeper penetration depth in biological tissues; (3) low photon energy of near-infrared laser minimizes photothermal damage to biomolecules and cells.<sup>25</sup> We did not observe considerable fluorescence background, and no “burning” effects are found in the sample area for the used laser power. In addition, the choice of the near-infrared excitation ensures that the SERS effects we detected are generated from the sharp edge of the nanocrescent moon, not the few residue nanospheres in our sample, since a near-infrared laser can hardly induce scattering peaks or plasmon resonance in nanospheres, which are necessary for the effective near-field energy transfer to adsorbed molecules.<sup>26,27</sup>

As shown in Figure 5a, 1  $\mu\text{M}$  is the lowest concentration that can be detected on the nanocrescent moon with our instruments. Assuming the cross-sectional area of the shown nanocrescent moon is about  $1 \times 10^{-7} \text{ mm}^2$ , there are only  $1 \times 10^{-20} \text{ mol}$  ( $\sim 6000$ ) R6G molecules on a nanocrescent moon after the uniform distribution of 1  $\mu\text{L}$  of 1  $\mu\text{M}$  R6G droplet (1 pico mol) on a  $\sim 10 \text{ mm}^2$  cross-sectional area, that is to say,  $\sim 6000$  R6G molecules can be detected on a single gold nanocrescent moon.<sup>28</sup> According to Nie et al.<sup>5</sup> and Kneipp et al.,<sup>6</sup> that the Raman scattering enhancement factor is above  $10^{14}$  for the single-molecule single-particle sensitivity, we estimate the Raman enhancement of a single gold nanocrescent moon could be higher than  $10^{10}$ . As a matter of fact, the enhancement factor could be higher because even fewer molecules are distributed close to the sharp edge area of the nanocrescent moon where most of the enhanced scattering signal is generated.

Though some characteristic peaks in the SERS spectrum of R6G molecules show only moderate enhancement on the nanocrescent moon (Figure 5b), the area of the “hot site” of a nanocrescent moon, the sharp edge, is smaller than that of the nanosphere clusters, their whole surfaces and thus the actual relative intensity enhancement per unit area should be higher than that shown in the plots. The relative intensity enhancement per unit area on the sharp edge of the nanocrescent moon is estimated larger than  $10^3$ , considering the nanosphere number ( $> 100$ ) within the laser excitation area.<sup>29</sup> On the other hand, some peaks are not visible on the gold nanospheres but are very distinct on the nanocrescent moon, especially for those vibrational peaks corresponding to aromatic ring bending and stretching, such as  $615 \text{ cm}^{-1}$ , which comes from the aromatic ring in-plane bending. In this case, the relative enhancement of the sharp edge compared to nanosphere clusters could be larger than  $10^5$ .<sup>29</sup> The reason for different enhancements to different Raman peaks by a single nanocrescent moon is not clear and under

further investigations. The Raman enhancement factor of an on-resonance Au nanosphere has been reported to be  $10^3 \sim 10^4$  using 514 nm laser excitation.<sup>30</sup> This enhancement factor is much smaller than that obtained from our single on-resonance nanocrescent moon, which is also supported by the simulation results from us and others.<sup>31</sup> Due to the interparticle plasmon coupling, the plasmon resonance wavelength of a cluster of Au nanospheres could shift to the range of near-infrared light and the nanospheres can be on-resonance using an NIR laser excitation. As reported before, an 830 nm laser excitation source was used and a Raman enhancement factor of  $\sim 10^9$  was obtained.<sup>30</sup> However, because of the random pattern of nanoparticle aggregations, the Raman enhancement factors are very different from place to place on an Au nanosphere cluster. A strong Raman enhancement could be obtained from particular positions on an Au nanosphere cluster after many trials in an unpredictable way. In contrast, the plasmon resonance of our nanocrescent moon is controllable and predictable because we intentionally design and fabricate it. On the other hand, the Raman enhancement effect of a single nanocrescent moon does not depend on the coupling between multiple particles, which makes the single nanocrescent moon an individual SERS substrate.

The sub-10 nm sharp edge of gold nanophotonic crescent moons incorporates the advantages of both metallic sharp nanotips and ultrathin nanorings, and generates local electromagnetic field enhancement. The fabrication of unconventional sharp-edged gold nanocrescent moons is accomplished by self-assembly of sacrificial nanospheres and conventional thin film deposition method without using e-beam, which allows batch nanofabrication process. We detected R6G molecules (about 6000 molecules) on a single gold nanophotonic crescent moon through the NIR laser-induced SERS spectroscopy, and the estimated Raman enhancement factor is larger than  $10^{10}$ . Based on the presented results, the sharp-edge gold nanophotonic crescent moons promise potential uses in ultrasensitive Raman, biomolecule and cellular imaging, and molecular medicine.

**Acknowledgment.** The Authors thank Dr. Y. Yin and Prof. A. P. Alivisatos for their technical support on transmission electron microscopy. This research was supported by grants to Y.L. from Samsung Research Fund and Nanophotonic Bioscience Fund, G.L. and J.K. from Intel Research Fund, and L.P.L. from NSF Career Award.

**Note Added after ASAP Publication.** Additional text was given for the Acknowledgment. This paper was published ASAP on 12/8/04. The corrected version was posted on 12/13/04.

## References

- (1) Mukerji, I.; Sipher, M. C.; Spiro, T. G.; Fresco, J. R. *Biochemistry* **1995**, *34*, 14300.
- (2) Chen, Y.-Q.; Kraut, J.; Callender, R. *Biophys. J.* **1997**, *72*, 936.
- (3) Fleischman, M.; Hendra, P. J.; McQuillan, A. J. *Chem. Phys. Lett.* **1974**, *26*, 123.
- (4) Lyon, L. A.; Keating, C. D.; Fox, A. P.; Baker, B. E.; He, L.; Nicewarner, S. R.; Mulvaney, S. P.; Natan, M. J. *Anal. Chem.* **1998**, *70*, 341R.
- (5) Nie, S.; Emory, S. R. *Science* **1997**, *275*, 1102.

- (6) Kneipp, K.; et al. *Phys. Rev. Lett.* **1997**, *78*, 1667.
- (7) Wang, Z.; Pan, S.; Krauss, T. D.; Du, H.; Rothberg, L. J. *PNAS* **2003**, *100*, 8638.
- (8) Oldenburg, S. J.; Jackson, J. B.; Wescott, S. L.; Halas, N. J. *Appl. Phys. Lett.* **1999**, *75*, 2897.
- (9) Jackson, J. B.; Halas, N. J. *J. Phys. Chem. B* **2001**, *105*, 2743.
- (10) Cao, Y. C.; Jin, R.; Mirkin, C. A. *Science* **2002**, *97*, 1536.
- (11) Bohren, C. F.; Huffman, D. R. *Absorption and Scattering of Light by Small Particles*; John Wiley & Sons Inc.: New York, 1998.
- (12) García-Vidal, F. J.; Pendry, J. B. *Phys. Rev. Lett.* **1996**, *77*, 1163.
- (13) Jensen, T. R.; Schatz, G. C.; Van Duyne, R. P. *J. Phys. Chem. B* **1999**, *103*, 2394.
- (14) Genov, D. A.; Sarychev, A. K.; Shalaev, V. M.; Wei, A. *Nano Lett.* **2004**, *4*, 153.
- (15) Crozier, K. B.; Sundaramurthy, A.; Kino, G. S.; Quate, C. F. *J. Appl. Phys.* **2003**, *94*, 4632.
- (16) Hayazawa, N.; Tarun, A.; Inouye, Y.; Kawata, S. *J. Appl. Phys.* **2002**, *92*, 6983.
- (17) Hartschuh, A.; Sanchez, E. J.; Xie, X. S.; Novotny, L. *Phys. Rev. Lett.* **2003**, *90*, 95503.
- (18) Aizpurua, J.; Hanarp, P.; Sutherland, D. S.; Kall, M.; Bryant, W.; Garcyá de Abajo, F. J. *Phys. Rev. Lett.* **2003**, *90*, 057401.
- (19) Love, J. C.; Gates, B. D.; Wolfe, D. B.; Paul, K. E.; Whitesides, G. M. *Nano Lett.* **2002**, *2*, 891.
- (20) Charnay, C.; Lee, A.; Man, S.-Q.; Moran, C. E.; Radloff, C.; Bradley, R. K.; Halas, N. J. *J. Phys. Chem. B* **2003**, *107*, 7327.
- (21) Glass slides were thoroughly rinsed with deionized water (Millipore, > 18 M $\Omega$ ) and dried under a stream of nitrogen gas. A thin layer of photoresist (Shiplacey S1818, Shiplacey, MA) was spin-coated on the cleaned glass substrates. Aqueous solutions of polystyrene colloids (300 nm; Duke Scientific, CA) were diluted in water to a volume fraction of 0.1%. A monolayer of sacrificial nanospheres was generated by drop-casting the dilute solution of the polystyrene colloids and allowed to dry overnight in a clean zone hood to minimize contamination of the samples by dust, and to stabilize the rate of evaporation. After the arrays of beads dried, a thin gold film was deposited by conventional electron beam evaporation. The sample substrate was placed above the gold source with certain tilt angle ( $\sim 30^\circ$ ), and the angle can be adjusted ranging from  $0^\circ$  to  $45^\circ$ . The substrate rotates at a constant speed ( $\sim 60$  rpm) during the deposition. The thickness at the bottom of the bowl is measured using TEM to be  $\sim 100$  nm. The shape of nanocrescent moons depends on the deposition thickness, angle, and the size of the sacrificial nanosphere template. The gold-coated colloids were released from the glass support into an aqueous suspension by lift-off with acetone. Next the gold-coated polymer nanospheres were collected by centrifugation ( $\sim 5000$  rpm, 5–10 min) and were suspended in toluene to dissolve the polystyrene. The sample was then centrifuged and washed 3–4 times in water. The gold nanocrescent moons were collected and resuspended in water or ethanol to form diluted colloids that were subsequently dropped on a  $100 \mu\text{m}$  thick glass substrate for spectrum measurement.
- (22) Johnson, P. B.; Christy, R. W. *Phys. Rev. B* **1972**, *6*, 4370.
- (23) A microscopy system combining dark-field scattering imaging and Raman spectroscopy is used to find “hot spots” and acquire Raman scattering spectra of R6G molecules adsorbed on a single gold nanocrescent moon. The system consist of a Carl Zeiss Axiovert 200 inverted microscope (Carl Zeiss, Germany) equipped with a dark-field condenser ( $1.2 < \text{NA} < 1.4$ ), a true-color digital camera (CoolSNAP cf, Roper Scientific, NJ), and a 300 mm focal-length monochromator (Acton Research, MA) with a  $1024 \times 256$ -pixel cooled spectrograph CCD camera with compensation in ultraviolet and near-infrared region (Roper Scientific, NJ). A  $2 \mu\text{m}$  wide aperture is placed in front of the entrance slit of the monochromator to keep only a single nanocrescent moon in the region of interest. The true-color scattering images of gold nanocrescent moons are taken using a  $60\times$  objective lens ( $\text{NA} = 0.8$ ) and the true-color camera with a white light illumination by a 100 W halogen lamp. The scattering spectra of gold nanocrescent moons are taken in visible light and infrared light regions separately, normalized with respect to the spectrum of a nonresonant nanoparticle (i.e., polystyrene) after the subtraction of background, then combined and normalized to unity. A 785 nm diode laser is used in our experiments as the excitation source of Raman scattering, and the laser beam (after attenuating neutral density filter) is focused by the same objective lens on single nanocrescent moon. The scattering and reflection light is then collected through the same optical pathway as the incident light and then through two 797 nm long-pass Raman filters (optical density > 6 below 797 nm and transmission > 90% above 800 nm, Omega Filters, VT). The Raman scattering light is resolved by a blaze grating of 300 grooves/mm and imaged by the spectrograph CCD.
- (24) Mertens, H.; Verhoeven, J.; Polman, A.; Tichelaar, F. D. *Appl. Phys. Lett.* **2004**, *85*, 1317.
- (25) Kneipp, K.; Haka, A. S.; Kneipp, H.; Badizadegan, K.; Yoshizawa, N.; Boone, C.; Shafer-Peltier, K. E.; Motz, J. T.; Dasari, R. R.; Feld, M. S. *Appl. Spectrosc.* **2002**, *56*, 150.
- (26) Michaels, A. M.; Nirmal, M.; Brus, L. E. *J. Am. Chem. Soc.* **1999**, *121*, 9932.
- (27) Kneipp, K.; Kneipp, H.; Kartha, V. B.; Manoharan, R.; Deinum, G.; Itzkan, I.; Dasari, R. R.; Feld, M. S. *Phys. Rev.* **1998**, *E57*, R6281.
- (28) We assume the nanocrescent moon (300 nm inner diameter and 100 nm bottom thickness) has a cross-sectional area an equivalent (slightly smaller) to a 400 nm in diameter nanosphere. The total cross-sectional area is  $\pi \times 200^2 \text{ nm}^2 = 1.26 \times 10^{-7} \text{ mm}^2$  ( $\sim 1 \times 10^{-7} \text{ mm}^2$ ), so the number of R6G molecules staying on the nanocrescent moon after drying is about  $1 \text{ pM} \times 6.02 \times 10^{23} \text{ M}^{-1} \times (1 \times 10^{-7} \div 10) = 6020$  ( $\sim 6000$ ).
- (29) The total cross-sectional area of 100 60 nm nanospheres is  $100 \times \pi \times 60^2 \text{ nm}^2 = 1.13 \times 10^{-6} \text{ mm}^2$ . As a conservative assumption, the cross-sectional area of the sharp edge is smaller than 1% of the whole nanocrescent moon, that is,  $1 \times 10^{-7} \text{ mm}^2 \div 100 = 1 \times 10^{-9} \text{ mm}^2$ , so the relative Raman peak intensity per unit area on the sharp edge of a gold nanocrescent moon can be 1000 times higher than that of 100 60 nm nanospheres if the total Raman peak intensities from both the single nano-crescent moon and nanosphere clusters are equivalent. The peak intensity at  $615 \text{ cm}^{-1}$  on the nanocrescent moon is at least 100 times larger than that on the nanospheres, so a relative enhancement factor of above  $10^5$  can be obtained.
- (30) Kneipp, K.; Kneipp, H.; Manoharan, R.; Hanlon, E. B.; Itzkan, I.; Dasari, R. R.; Feld, M. S. *Appl. Spectrosc.* **1998**, *52*, 1493.
- (31) Kelly, K. L.; Coronado, E.; Zhao, L. L.; Schatz, G. C. *J. Phys. Chem. B* **2003**, *107*, 668.

NL048232+